# Scanning dynamic light scattering optical coherence tomography for measurement of high omnidirectional flow velocities

Cheishvili, Konstantine; Kalkman, Jeroen

**DOI**
10.1364/OE.456139

**Publication date**
2022

**Document Version**
Final published version

**Published in**
Optics Express

**Citation (APA)**
Cheishvili, K., & Kalkman, J. (2022). Scanning dynamic light scattering optical coherence tomography for measurement of high omnidirectional flow velocities. *Optics Express*, *30*(13), 23382-23397. https://doi.org/10.1364/OE.456139

**Important note**
To cite this publication, please use the final published version (if applicable).
Please check the document version above.

Research Article | Vol. 30, No. 13 / 20 Jun 2022 / Optics Express 23382
Optics EXPRESS

# Scanning dynamic light scattering optical coherence tomography for measurement of high omnidirectional flow velocities

KONSTANTINE CHEISHVILI* AND JEROEN KALKMAN

*Department of Imaging Physics, Delft University of Technology, Lorentzweg 1, 2628 CJ Delft, The Netherlands*
*k.cheishvili@tudelft.nl

**Abstract:** We show scanning dynamic light scattering optical coherence tomography (OCT) omnidirectional flow measurements. Our method improves the velocity measurement limit over conventional correlation-based or phase-resolved Doppler OCT by more than a factor of 2. Our technique is applicable without a-priori knowledge of the flow geometry as our method works both for non-zero Doppler angle and non-ideal scan alignment. In addition, the method improves the particle diffusion coefficient estimation for particles under flow.



## 1. Introduction

Dynamic light scattering optical coherence tomography (DLS-OCT) relies on the measurement of fluctuations of scattered light and coherence gating to obtain simultaneous depth-resolved information about diffusive and translational motion of particles. This information is extracted from the temporal autocorrelation of the OCT signal for every voxel in depth. Initially, DLS-OCT was used for particle sizing [1] where the particle size is determined from the estimated diffusion coefficient using the Stokes-Einstein relation.

Flow measurements with OCT have been performed using phase-resolved Doppler OCT, lateral resonant Doppler OCT [2], and M-scan correlation-based DLS-OCT [3–5]. The axial velocity of Doppler OCT is limited by phase wrapping. In the correlation-based measurements, the maximum transverse velocity is limited by the decorrelation rate, which depends on the spatial resolution of the system [6]. The axial velocity range is limited by interference fringe washout [7] and the coherence length of the source. When measuring the diffusion of particles under flow, the decorrelation in the flow causes uncertainty in the estimated diffusion coefficient [8], which, in case of high flows, cannot be measured at all.

In this work we apply beam scanning in DLS-OCT to improve the maximum measurable velocity limit for omnidirectional flows. We extend the existing theoretical models [3,9] for the OCT signal autocorrelation and incorporate the motion of the beam into it. We show that when scanning the OCT beam in the direction of the flow, the dynamic velocity range is significantly increased. We demonstrate that the B-scan correlation-based DLS-OCT method is capable of measuring a far higher range of velocities than standard Doppler OCT, lateral resonant Doppler OCT [2] or conventional correlation analysis (M-scan) with stationary beam.

## 2. Theory

### 2.1. Sample geometry

The geometry for OCT flow measurements is shown in Fig. 1(a). The propagation of the optical beam is in the $z$ direction. The flow is in a channel oriented at an angle $\alpha$ with respect to the $x$-$y$ plane. This angle can, due to refraction of the light, be different from the orientation of the flow direction at angle $\theta$. In general, we assume the flow to be laminar with transverse, $v_t(z)$, and axial, $v_z(z)$, velocity components as a function of depth. Given a total flow $v_0(z)$, the flow components

#456139 https://doi.org/10.1364/OE.456139
Journal © 2022 Received 15 Feb 2022; revised 14 Apr 2022; accepted 16 Apr 2022; published 13 Jun 2022

Optics EXPRESS

are expressed as $v_t(z) = v_0(z)\cos\theta$ and $v_z(z) = v_0(z)\sin\theta$. The OCT beam is a Gaussian beam characterized by the waist $w_0$ in focus, defined as a distance from the beam center where the field amplitude is $e^{-1}$ of its maximum value. The OCT beam can be scanned in the direction of the flow with speed $v_b$ in the $x$-$y$ plane. The 3D scan speed along the flow is $v_s$, which, in general ($\theta \neq 0°$), is larger, than $v_b$. The more general case of 3D flow measurements with scanning OCT is shown in Fig. 1(b-d). Here $\varphi_t$ is the angle between projections of the scan and flow vectors in the transverse plane, and $\varphi_z$ is the difference between the angles that the scan and flow vectors make to their corresponding transverse projections.

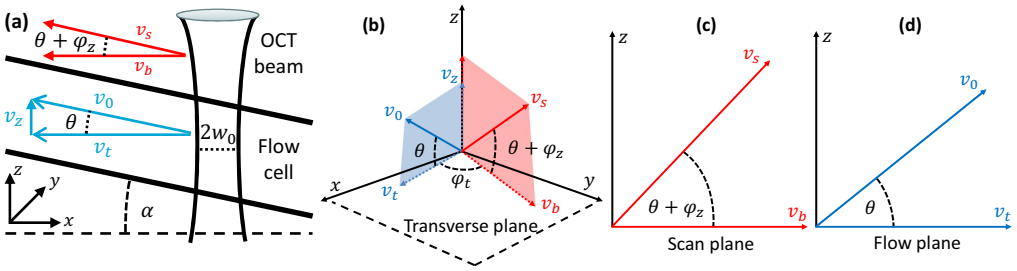


**Fig. 1.** Geometry of the flow and the scanning OCT setup. (a) The flow and the OCT beam layout. (b) The flow vectors in the flow plane (blue) and scan vectors in the scan plane (red). (c) The scan plane with scan vector and its transverse projection. (d) The flow plane with flow vector and its transverse projection.

Quantitative OCT flow measurements have been performed with different techniques. Here we discuss four different techniques, namely

- M-scan Doppler OCT
- B-scan Doppler OCT
- M-scan DLS-OCT
- B-scan DLS-OCT

where the last method is the new method developed by us.

### 2.2. M-scan Doppler OCT

The most used method for measuring the axial flow velocity is phase-resolved Doppler OCT. Due to the Doppler effect, the frequency of light scattered from a particle undergoing axial motion is shifted. The Doppler shift in the scattered light leads to a phase change of the OCT signal, $\Delta\phi(z)$. From the phase change the axial depth-resolved velocity $v_z(z)$ is determined using [10]

$$v_z(z) = \frac{\Delta\phi(z)}{q\Delta t}, \tag{1}$$

where $\Delta t$ is the sampling time, and $q = 2nk_0$ is the scattering wavenumber for the backscattering probe configuration with the medium refractive index $n$ and the vacuum wavenumber $k_0$. The total and axial flow velocities are related with the expression $v_0(z) = v_z(z)/\sin\theta$. The maximum velocity that can be estimated using Eq. (1) is limited by the Nyquist sampling criterion as

$$v_{z_{\max}} = \frac{\pi}{q\Delta t}. \tag{2}$$

However, Eq. (2) is only true for flows at low transverse velocity [10]. At high transverse velocities, because of the changing intensity of the illuminating beam on the moving particles,

Optics EXPRESS

the phase change does not increase linearly with the velocity and approaches a constant value. This makes it impossible to determine the velocity for high lateral flow speeds.

### 2.3. B-scan Doppler OCT

As Koch et al. highlighted, transverse movements during the detector integration time as small as 20% of the beam diameter can lead to erroneous velocity measurements [10]. To correct for the deviation from Eq. (1) due to the short transit time of the particle through the beam, Walther and Koch suggested a method of laterally scanning the beam along the flow and performing the Doppler analysis on numerically aligned OCT data [2]. Synchronizing the OCT beam movement with the direction of the flow reduces the effective transverse velocity and its effect on the phase shift. While this method can be quite effective with uniform flows, its usability is reduced for flows where the transverse velocity components vary over depth. In that case, the transverse velocity effects cannot be fully suppressed for all depths using a single B-scan.

### 2.4. M-scan DLS-OCT

While the Doppler methods only can determine axial flows, correlation-based DLS-OCT methods can be used to determine both axial and transverse flows. For a Gaussian illuminating beam and Gaussian-shape spectral envelope, the depth-dependent autocovariance of the OCT complex signal in a backscattering geometry is given by [3,4,8,9]

$$g_1(z,\tau) = A_1(z)\mathrm{e}^{iqv_z(z)\tau}\mathrm{e}^{-Dq^2\tau}\mathrm{e}^{-\frac{v_z(z)^2\tau^2}{2w_z^2}}\mathrm{e}^{-\frac{v_t(z)^2\tau^2}{w_0^2}}, \tag{3}$$

where $D$ is the diffusion coefficient, $w_z$ is the coherence function waist ($\mathrm{e}^{-1}$ distance) in the sample, and $\tau$ is the correlation time lag. For the Gaussian source spectrum with a wavenumber standard deviation $\sigma_k$ and the sample refractive index $n$ the coherence function waist is given by $w_z^{-1} = \sqrt{2}\sigma_k n$. The parameter $A_1(z)$ is the autocovariance amplitude containing the effect of a diminishing signal-to-noise in depth [11] and takes values between 0 and 1. Note that the decorrelation only depends on the in-focus beam radius $w_0$ [8,12,13] which makes depth-dependent analysis relatively straightforward. The decorrelation of the OCT signal magnitude is a factor two higher [1,8] than the field decorrelation and can be expressed with the second-order autocovariance [14,15]:

$$g_2(z,\tau) = |g_1(z,\tau)|^2 = A_2(z)\mathrm{e}^{-2Dq^2\tau}\mathrm{e}^{-\frac{v_z(z)^2\tau^2}{w_z^2}}\mathrm{e}^{-\frac{2v_t(z)^2\tau^2}{w_0^2}}, \tag{4}$$

where $A_2(z)$ is a depth-dependent amplitude factor. Equation (4) is valid with the assumption that the average number of particles in the scattering volume, $N$, is sufficiently large ($N \gtrsim 100$) [12,14,16].

In this paper we focus on the second-order autocovariance function, $g_2(z,\tau)$, that does not depend on phase, is easier to implement, and can also be implemented in phase-unstable OCT systems. When the autocovariance function is used for estimating the flow, the $\mathrm{e}^{-1}$ decay time of the autocorrelation must be equal or larger than the temporal sampling time $\Delta t$. From this requirement, the maximum measurable transverse and axial flow speeds are

$$v_{t_{\max}} = \frac{w_0}{\sqrt{2}\Delta t}, \tag{5}$$

$$v_{z_{\max}} = \frac{w_z}{\Delta t}, \tag{6}$$

respectively. These equations are derived under the assumption of ideal $\delta$-function sampling. However, when the measurements are performed while integrating over a specific detector time,

Optics EXPRESS

defined by $T = \Delta t/C$ (where $C$ is the multiplicative constant larger or equal to 1), the axial motion of a sample during the integration time causes a significant SNR degradation that limits the axial velocity to

$$v_{z_{\max}} = \frac{\pi C}{q\Delta t}\,. \tag{7}$$

Eqs. (5) and (6) limit the maximum measurable transverse and axial velocity components from a correlation perspective: when the effective particle displacements become comparable to the transverse and axial resolutions, the acquired signals become completely decorrelated within a single acquisition time [6]. Equation (7) limits the axial velocity due to fringe washout at the detector [7]. For the spectrometer-based OCT systems, the detector integration time is comparable to the sampling time, i.e, $C \gtrsim 1$. Such systems operate in the visible and infrared wavelength ranges with $q/\pi \gg w_z^{-1}$, therefore limiting the axial velocity by the fringe washout through Eq. (7), rather than by the axial resolution through Eq. (6).

### 2.5. B-scan DLS-OCT

To circumvent the limit imposed by Eq. (5) we propose the implementation of flow quantification using B-scan correlation-based DLS-OCT. When moving the OCT beam in any direction with a constant velocity while acquiring the signal, $v_t(z)$ and $v_z(z)$ in Eq. (4) must be replaced with the effective transverse $\Delta v_t(z)$ and axial $\Delta v_z(z)$ velocities, given by

$$\begin{aligned}\Delta v_t(z)^2 &= [v_0(z)\cos\theta - v_s\cos\varphi_t\cos(\varphi_z+\theta)]^2 + [v_s\sin\varphi_t\cos(\theta+\varphi_z)]^2\\ &= v_0(z)^2\cos^2\theta - 2v_0(z)v_s\cos\varphi_t\cos\theta\cos(\theta+\varphi_z) + v_s^2\cos^2(\theta+\varphi_z),\end{aligned} \tag{8}$$

$$\Delta v_z(z)^2 = [(v_0(z)\sin\theta - v_s\sin(\theta+\varphi_z)]^2\,, \tag{9}$$

where $v_s$ is the effective scan speed in 3D along the flow, $\varphi_t$ and $\varphi_z$ are the angles defining the scan direction relative to the flow, shown in Fig. 1(a-d). When the effective scan direction is sufficiently aligned with the flow velocity, so that $\cos\varphi_t \approx 1$ and $\theta + \varphi_z \approx \theta$, Eq. (8) and (9) are simplified into

$$\Delta v_t(z) = (v_0(z) - v_s)\cos\theta = \Delta v_0(z)\cos\theta, \tag{10}$$

$$\Delta v_z(z) = (v_0(z) - v_s)\sin\theta = \Delta v_0(z)\sin\theta\,, \tag{11}$$

which shows that with an ideal scan alignment, the ratio of the effective transverse and axial velocity components remains unchanged irrespective of the beam scan speed $v_s$. This simplification allows calculation of flow velocities by adding effective flow and scan speeds. Therefore, an autocovariance model of the OCT signal magnitude for the general case of beam scanning incorporating the beam motion can be written as

$$g_2(z,\tau) = A_2(z)\mathrm{e}^{-2Dq^2\tau}\mathrm{e}^{-\frac{(v_0(z)-v_s)^2\sin^2\theta\,\tau^2}{w_z^2}}\mathrm{e}^{-\frac{2(v_0(z)-v_s)^2\cos^2\theta\,\tau^2}{w_0^2}}\,, \tag{12}$$

with the limitation that the axial intensity profiles are the same for all lateral B-scan acquisitions. For Eq. (12), the axial velocity limit is unchanged and limited by the fringe washout via Eq. (7). However, the transverse velocity limit is modified; Eq. (5) is now limited by the relative velocity $\Delta v_t$ rather than the absolute velocity $v_t$. This implies that for flows uniform along the length of the B-scan, the maximum measurable flow is limited by the absolute difference between flow and scan speeds. The application of lateral scanning in correlation analysis can give a significant improvement because for a typical OCT flow geometry the transverse flow is much higher than the axial flow and the limitation caused by the transverse flow, Eq. (5), is more restrictive than that for axial flow, Eq. (7). For a flow profile $v_t(z)$ the most optimum scan speed is such that the decorrelation rate is at its maximum for the highest and lowest flows, i.e., the effective scan

Optics EXPRESS

speed $v_s$ is a mid-range flow velocity $v_s \cos\theta = \frac{\max[v_t(z)]+\min[v_t(z)]}{2}$. This scan speed will cause maximum and equal decorrelation rates for the maximum and minimum flow speeds. Hence, with optimal scan speed, the maximum transverse velocity is limited to

$$v_{t_{\max,B}} = \frac{\sqrt{2}w_0}{\Delta t} + \min[v_t(z)]\,, \tag{13}$$

or stated differently,

$$v_{t_{\max,B}} = 2 \cdot v_{t_{\max,M}} + \min[v_t(z)]\,, \tag{14}$$

which shows that for measuring flow profiles where a minimum velocity is zero, the B-scan flow measurement limit is a factor of 2 larger than the conventional M-scan DLS-OCT flow limit. This equation is valid within the small angle approximation between scan and flow vectors. However, to obtain the actual flow speeds, the effective scan speed needs to be added to the velocities determined with correlation after acquisition. For flows with a non-uniform transverse component, assuming that the beam can be moved at sufficiently high velocities, the maximum flow that can be determined with B-scanning is at least twice the flow that can be determined without. However, this has no effect on the axial velocity limit imposed by the fringe washout.

## 3. Materials and methods

### 3.1. OCT system

The experiments were performed using a Thorlabs GANYMEDE II HR series spectral domain OCT System, with a bandwidth centered around 900 nm with an axial resolution of $l_c = 3$ µm in air. The OCT system was operated both in M-scan and B-scan modes. In M-scan mode, subsequent A-scans were acquired at a fixed sample position. In B-scan mode, the beam was moved in the transverse plane, perpendicular to the illumination direction, while acquiring A-scans. Because of the telecentric scan arrangement, the scanned beam remains perpendicular to the transverse plane for all lateral positions. The acquisition rate was set at 36 kHz for all experiments. The OCT axial resolution and axial decorrelation were determined using the wavenumber spectrum standard deviation, $\sigma_k$, of the measured reference spectrum. The acquired signal spectrum was measured with a spectrometer with 2048 pixels. After acquisition, the measured spectrum was resampled to a linearly-sampled wavenumber domain and apodized using a Gaussian filter. After the apodization, the measured axial resolution and coherence function waist in sample were $l_c = 4$ and $w_z = 2.5$ µm, respectively.

The OCT system is operated with a scan lens (LSM04-BB, Thorlabs) in a confocal setup with a focal spot size of $w_0 = 6$ µm in air, defined as the $e^{-1}$ radius of the field function. The NA of the system was 0.05. The manufacturer-provided waist size in air was validated by measuring the axial confocal response of a reflector moving through the beam focus. The measured values were around $w_0 = 5 - 6$ µm. However, depending on the angle of incidence, refractive index contrast and Gaussian beam parameters, $w_0$ varies somewhat because of the passage of the beam through the interfaces [17]. Therefore, for each experiment, $w_0$ was calibrated by performing a B-scan with a known transverse scan speed on a static sample, and then fitting $w_0$ from Eq. (4) using the correlation analysis. This gave results similar as for the confocal measurement, but slightly lower ($w_0 = 4.5$ µm). For maximizing the number of particles within the scattering volume, the region of interest in the depth range was moved away from the focus by approximately 0.5 mm [12]. Since for the given OCT setup the coherence length and the NA are very low, it can be assumed that the scattering angle is 180° and the scattering wavenumber $q$ in the correlation analysis is constant at $q = 2nk_0$.

Optics EXPRESS

### 3.2. Flow system

The flow was generated using a syringe pump with variable discharge rate (Fusion 100, Chemyx) and a 60 mL syringe (BD Plastipak). The flow passes through a quartz rectangular flow cell with internal dimensions of 0.2 mm thickness and 10 mm width (type 45-F, Starna Scientific). For each experiment, the flowing sample consisted of 5 mL 20% Intralipid (Fresenius Kabi) solution dissolved in 200 mL water, resulting in a total particle volume fraction of approximately 0.5%. The refractive index of the solution was determined by measuring the OCT amplitude signal of the flow cell filled with the sample and numerically solving the following equation

$$\cos\left[\sin^{-1}\left(\frac{\sin\alpha}{n}\right)\right] = \frac{hn}{L}, \tag{15}$$

where $h$ is the known flow cell thickness, $L$ is the measured peak-to-peak optical path length difference between the flow cell surfaces, and $\alpha$ is the angle between the cuvette and a plane normal to the optical beam. The obtained refractive index was $n = 1.38$. As a reference, velocity profiles for the set pump discharge rates were calculated using the analytical solution for the Poiseuille flow in a rectangular channel [18]

$$v(y = \frac{w}{2}, z) = \frac{40 \cdot Q}{3\pi^3 hw(1 - 0.63\frac{h}{w})} \sum_{m=1,m\,\mathrm{odd}}^{\infty} \frac{\sin(\frac{m\pi z}{h})}{m^3}, \tag{16}$$

where the velocity, in mm/s, is given as a function of depth $z$ at the flow cell half-width, $w$ is a width of the flow cell and $Q$ is the pump discharge rate in mL/s. All flow cell dimensions are in mm. In the analytical solution, the maximum velocities are observed at the half-width of the cell. Therefore, the OCT beam was positioned as close as possible to this location. In the transverse plane, the flow and B-scan directions were aligned as good as possible. In the axial plane, the angle $\alpha$ was fitted to the surface as shown in Fig. 2 and numerical alignment was performed using the voxel-shifting technique.

### 3.3. M-scan OCT flow measurements

In the M-scan mode, depending on the expected flow velocities, the measurement time series lengths were chosen between $N = 240$ and $N = 2845$ matching the lengths of the associated B-scan lengths. Each M-scan measurement was repeated 100 times. The beam was stationary during the whole signal acquisition period.

#### 3.3.1. M-Scan Doppler OCT flow measurements

Axial velocities were determined using the depth-dependent and time-averaged phase changes from 240 – 2845 adjacent A-scans using Eq. (1) with

$$\Delta\phi(z) = \left\langle \tan^{-1}\left[\frac{\mathrm{Im}\big(a(z,t)\times a^*(z,t+\Delta t)\big)}{\mathrm{Re}\big(a(z,t)\times a^*(t,t+\Delta t)\big)}\right]\right\rangle_t, \tag{17}$$

where $a(z,t)$ and $a(z,t+\Delta t)$ represent the complex OCT data at times $t$ and $t+\Delta t$, respectively. Total flow velocities were determined by diving the axial velocities with $\sin\theta$.

#### 3.3.2. M-scan DLS-OCT flow measurements

The M-scan correlation analysis was performed by fitting the autocovariance function using only $v_0(z)$ and $A_2(z)$ as free parameters. Prior to fitting, several reference measurements were performed. First, an M-scan measurement was performed with only diffusion and no flow. The diffusion coefficient $D$ was determined from the fit of Eq. (4) to the autocovariance of the M-scan

Optics EXPRESS

OCT signal amplitude from the stationary fluid. This measurement was performed for every time series length from $N = 240$ to $N = 2845$ to account for the statistical bias in $D$ caused by the time series length [11]. The statistically corrected diffusion coefficient was subsequently used in all following analysis as a fixed parameter. Depending on the time series length, the measured diffusion coefficients were $1.47 - 3.80 \times 10^{-12}$ m$^2$/s.

Afterwards, one B-scan measurement was made under no-flow condition. From the a-priori known set B-scan velocity, the beam waist $w_0$ was determined using a fit of Eq. (4). Depending on the measurement, the obtained $w_0$ values were $4.26 - 4.51$ µm. The beam waist was used in all following analysis as a fixed parameter. In the last calibration step, the Doppler angle $\theta$ was determined by using $w_0$, $D$ and $v_z(z)$, obtained from the phase-resolved Doppler analysis, in combination with Eq. (4), fitting $v_t(z)$, and then finding the depth-averaged angle $\theta = \left\langle \arctan \frac{v_z(z)}{v_t(z)} \right\rangle_z$. This measurement was performed in M-scan mode using a low discharge rate to avoid phase wrapping. After the calibration, OCT M-scan flow measurements were performed. The total velocity, $v_0(z)$, was fitted using Eq. (4) on the averaged data, incorporating the calibrated $D$, $w_0$, and $\theta$.

### 3.4. B-scan OCT flow measurements

In B-scan mode, the OCT beam was scanned while acquiring the data. The length of a time series (the number of acquired A-scans) could not be set at will, but is dependent on the scan speed, the A-scan acquisition rate, and the scan distance. With the A-scan acquisition rate at 36 kHz and the scan distance fixed to 1 mm to ensure identical sample uniformity for all measurements, the time series consisted of 240 to 2845 successive A-scans for scan speeds of 12.7 to 150.8 mm/s, respectively. One M-scan measurement was performed for obtaining the background noise of the signal amplitude in the depth domain. This amplitude was subtracted from all measurements before the numerical alignment.

#### 3.4.1. B-Scan Doppler OCT flow measurements

The obtained signal was numerically aligned as described in Sec. 3.4.3. Afterwards, axial velocities were determined using the depth-dependent and time-averaged phase changes from Eq. (1). Total flow velocities were determined as in the M-scan Doppler mode. In the B-scan mode, the Doppler method suffered less from the effects of transverse velocities when using the depth-domain alignment compared to the frequency-domain alignment.

#### 3.4.2. B-scan DLS-OCT flow measurements for scanning along an in-plane flow

For B-scan correlation-based flow measurements, the transverse scan direction of the OCT beam was aligned to the flow direction as much as possible, with $\cos\varphi_t \approx 1$ and $\theta \approx \theta + \varphi_z$. In this limiting case the only fitting parameters are $v_0(z)$ and $A_2(z)$. The scan speed was chosen to be close to the expected mid-range velocity within the flow profile, calculated analytically from the pump discharge rate, the dimensions of the flow channel, and Eq. (16). The same calibration measurements were used as in the M-scan mode.

#### 3.4.3. B-scan DLS-OCT flow measurements for scanning along an out-of-plane flow

The application of B-scan DLS-OCT is most straightforward for a flow perpendicular to the beam. However, in the more general case of oblique flow, the same path length in the B-scan corresponds to different physical depths in the flow, and hence, direct implementation of the correlation analysis is not possible. Therefore, the data has to be numerically aligned to have identical sample locations on identical depths for all transverse points of the B-scan.

Numerical alignment is either achieved using a spatial shift of the OCT signal in the depth domain obtained after the inverse Fourier transformation of the spectrum, or, equivalently, by

Optics EXPRESS

using a phase multiplication in the frequency domain before the inverse Fourier transform. Figure 2 shows the numerical alignment process. In the depth-domain, the spatial shift is accomplished by circularly shifting depth voxels by an integer number $\Delta_z(t)$ as a function of time $t$ according to

$$\Delta_z(t) = \text{nint}\left(\frac{nv_b t \tan\alpha}{\delta z}\right), \tag{18}$$

$$I(z_j, t) \Longrightarrow I(z_{j+\Delta_z(t)}, t), \tag{19}$$

where $t$ is the acquisition time, $\alpha$ is a physical flow cell tilt angle, and $\delta z$ is the voxel size interval [19]. The rounding operation is necessary as the voxels can only be shifted by an integer number. Depending on the scan direction, the voxels are shifted upwards or downwards. A fully equivalent result can be obtained in the frequency domain using

$$I(k, t) \Longrightarrow I(k, t)\mathrm{e}^{-i2knv_b t\tan\alpha}, \tag{20}$$

$$I(k, t) \xrightarrow{\mathcal{F}^{-1}} I(z, t), \tag{21}$$

After aligning the scan and flow directions, the effective scan speed, $v_s$, is the effective speed at which the beam scans along the oblique flow. It is required for fitting Eq. (12) and can be expressed as

$$v_s = \frac{v_b}{\cos\alpha}. \tag{22}$$

The validity of the autocovariance model in Eq. (12) relies on the assumption of stationarity. This is only truly valid if the intensity fluctuations for any given depth voxel do not have an explicit dependence on time and that the average intensity remains constant. At non-zero tilt angles $\alpha$ these conditions are not met while B-scanning, because adjacent pixels correspond to different flow speeds and therefore are described by different random processes. The numerical re-alignment is performed to remedy this effect and make sure that adjacent pixels in time correspond to the same position in the flow channel and therefore have the same flow speeds. However, this process introduces a mismatch between the signal levels of adjacent pixels. First, the aligned pixels in time correspond to different locations within the axial confocal PSF. Second, due to the sensitivity roll-off the OCT signal is different for these pixels. Third, depending on the axial velocity distribution, the signal decay due to the fringe washout effect may also differ. Therefore, before performing the numerical re-alignment, at each lateral position, the OCT signal intensity was normalized with the averaged depth-dependent OCT signal at that location. It was assumed that for the normalization a sufficient number of B-scans was recorded to extinguish signal fluctuations due to particle motion.

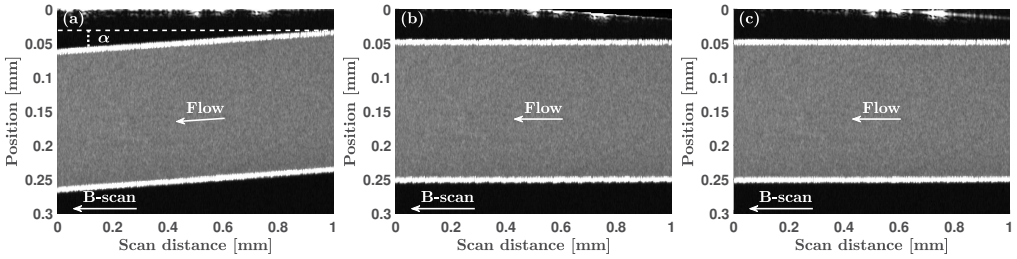


**Fig. 2.** OCT numerical image alignment. (a) Original depth-resolved B-scan image. (b) B-scan alignment in the spatial domain. (c) B-scan alignment in the frequency domain.

Figure 3 shows the processing steps for obtaining velocities. After numerically aligning the flow measurements, the autocovariance at a depth $z$ at the center of a flow cell, where the velocity

Optics EXPRESS

is highest was fitted using Eq. (12) using $D$, $w_0$, $w_z$ and $\theta$ as input parameters to obtain the effective velocity, as shown in Fig. 3(a). The B-scan autocovariance decays slower than the M-scan counterpart because the scan is along the flow. Noise decorrelates in a single time step, therefore, $g_2(h/2, \tau = 0)$ is omitted from the fit. The fitted autocovariance amplitude is slightly lower for the B-scan measurement. We attribute this to the fact that the transverse beam motion degrades the OCT signal [20].

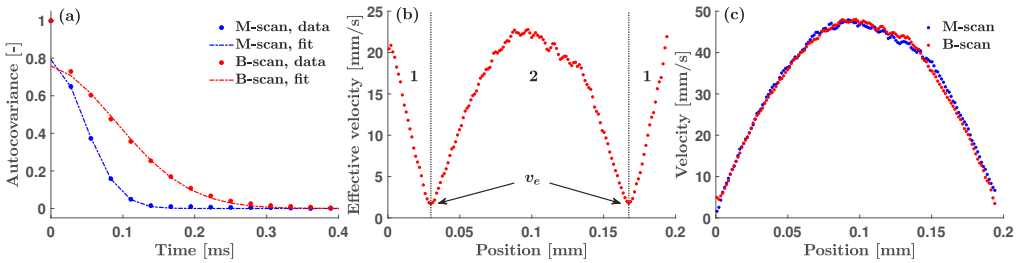


**Fig. 3.** (a) M-scan and B-scan correlation functions at $z = h/2$ with the flow rate 1/15 mL/s and $\theta = 0.39°$. (a) Measured autocovariance, $g_2(h/2, \tau)$. (b) Measured $\Delta v_0(z)$ from B-scan. (c) Measured and reconstructed $v_0(z)$ from both M-scan and B-scan analysis, respectively.

Figure 3(b) shows the obtained effective velocity for all depths in the flow channel. As can be seen the parabolic flow profile is mirrored at an effective velocity close to zero. The jitter velocity $v_e$ causes the "dips" in the flow velocity profile to have a small offset. For B-scan correlation analysis, the fitted velocity is the difference between the flow and effective scan speeds, or the effective velocity, $\Delta v_0$. The flow velocity $v_0(z)$ was then obtained using

$$(v_0(z) - v_s)^2 + v_e^2 = \Delta v_0(z)^2 \,, \tag{23}$$

with $v_s$ the scan velocity along the flow and $v_e$ a non-zero fitted velocity when $v_s = v_0(z)$. Ideally, with a well-calibrated diffusion coefficient and the beam motion perfectly aligned with the flow, it is expected from the Eq. (10)–(12) that $v_e = 0$. However, due to small scan misalignments, galvo instability, and jitter there is additional decorrelation that leads to an offset $v_e$. Since $v_e$ is much smaller than $v_s$ and $v_0(z)$ it is only observed as $v_0(z) \approx v_s$. Therefore, $v_e$ is obtained as the average of both minima from Fig. 3(b). After finding $v_e$, $v_0(z)$ is determined by solving the quadratic Eq. (23). This equation has two solutions that are mirror reflections over the line where the effective velocity equals $v_s$. To find the correct value the velocity profile is split into two regions. In the region 1 the flow speed is lower than the effective scan speed, while in the region 2 the flow speed is higher than the effective scan speed. So, the solution $v_0(z) < v_s$ is chosen for the region 1 and the solution $v_0(z) > v_s$ is chosen for the region 2. Equation (23) can also be solved explicitly, i.e., without any assumptions for $v_0(z)$ or $v_e$, if two or more B-scans are performed at different speeds for the same flow velocities.

Figure 3(c) shows the obtained full flow profile compared to the flow profile measured with M-scan DLS-OCT. Clearly, the same flow profile is obtained.

#### 3.4.4. B-scan DLS-OCT flow measurements for arbitrary scan direction and out-of-plane flow

The most general application of our method is under the condition that the flow is not in the transverse plane and that the B-scan angle is not exactly aligned with the transverse flow direction. In this case flow measurements were performed in the B-scan mode similar to the aligned condition. The scan distance was kept the same but the measurement averaging was increased from 100 to 200 scans. No assumptions were made for the angles $\varphi_t$ and $\varphi_z$. The scan direction was at an angle of about $\varphi_t \approx 10°$ from the flow direction. In this case, only the background noise

Optics EXPRESS

and the beam waist calibration measurements were performed. For each flow speed, B-scans at 5 different scan speeds were acquired. Due to the purposeful misalignment, flow and scan vectors never fully match and the decorrelation rate was nonzero for every depth. Since the diffusive term is only important when the scan and flow velocities coincide (yielding low decorrelation), it was neglected here. For every acquired B-scan a total decorrelation rate $\Gamma(z)$ was obtained by fitting

$$g_2(z,\tau) = A_2(z)\mathrm{e}^{-\Gamma(z)\tau^2} \tag{24}$$

to the depth-resolved OCT signal amplitude, with

$$\Gamma(z) = \frac{\Delta v_z(z)^2}{w_z^2} + \frac{2\Delta v_t(z)^2}{w_0^2}\,, \tag{25}$$

with $\Delta v_t(z)$ and $\Delta v_z(z)$ defined in Eq. (8) and (9). First, $\Gamma(z)$ is fitted for all five B-scan measurements at all depths. Second, an overdetermined system of equations is constructed with unknowns $v_0(z)$, $\theta$, $\varphi_t$ and $\varphi_z$. The total number of equations equals five times the number of samples in depth. Finally, the system of equations is solved simultaneously for all depths using a nonlinear least-squares method, yielding the values for $v_0(z)$, $\theta$, $\varphi_t$ and $\varphi_z$.

## 4. Experimental results

### 4.1. Flow measurements under ideal scanning alignment

Three sets of flow measurements were performed for $\theta$ values of 0.39°, 0.94° and 1.58°. For each angle, the pump discharge rates were varied from 1/30 to 1/3 mL/s. Figure 4 shows velocity profiles obtained with M-scan Doppler OCT, M-scan DLS-OCT, B-scan Doppler OCT, and B-scan DLS-OCT, where each column corresponds to the same method. For improved data visibility, only the profiles with less than 20% relative error between the expected and measured integrated flow profiles, as well as less than 20% relative mean squared error with respect to the expected velocity profiles, are shown. Dashed parabolic curves are the theoretical velocities at the center of the cuvette, while the horizontal lines represents the maximum velocities that can be measured by any given method.

Figure 4(a,e,i) shows the M-scan Doppler OCT flow measurements. With increasing discharge rate, the phase shift approaches a constant value due to phase distortion and the profiles become inaccurate, which is consistent with the results from Koch et al. [10]. At larger angles the Doppler flow becomes less noisy. Since the flow cell is oriented almost perpendicular to the beam optical axis, the axial velocity is proportional to the Doppler angle ($\sin\theta \approx \theta$), while the transverse velocity is almost unaffected by the angle ($\cos\theta \approx 1$). The M-scan Doppler OCT has the lowest velocity dynamic range, for the current settings limited to 51 mm/s. Using simulations based on the models from [10], expected velocities at which the phase shifts, for the given geometry, deviate from the linear phase increment are above 50 mm/s, which is consistent with our observations.

Figure 4(b,f,j) shows the M-scan DLS-OCT flow measurements. Depending on the Doppler angle, the maximum velocity is 101-127 mm/s. The expected maximum velocity from Eq. (5) and (6) is approximately 115 mm/s, which is consistent with our observations. The velocity values become more noisy for higher discharge rates. In this case the velocity limit is dictated by Eq. (5) and (6), because the fringe washout limit has not been reached. The maximum measurable velocity slightly decreases with increasing $\theta$. This is expected, since the coherence function waist is slightly smaller than the Gaussian beam waist. Therefore, for the same flow rate, the decorrelation becomes more rapid with increasing axial velocity. This method has a higher velocity limit compared to M-scan Doppler OCT. The flow limit for M-scan DLS-OCT is approximately a factor 2 higher than for M-scan Doppler OCT.

Optics EXPRESS

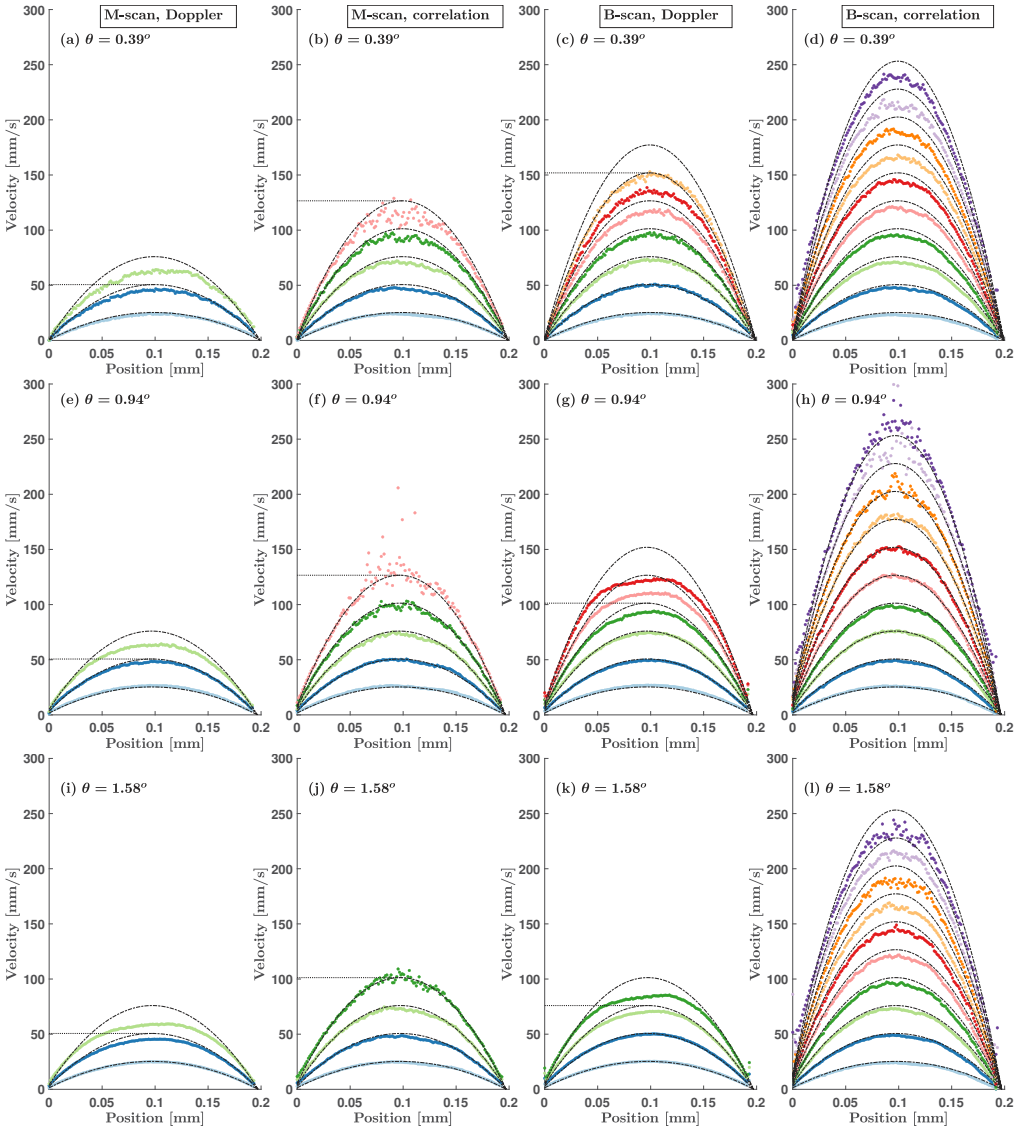


**Fig. 4.** Flow profiles measured using different methods (columns) and angles (rows). (a-d) $\theta = 0.39°$. (e-h) $\theta = 0.94°$. (i-l) $\theta = 1.58°$.

Optics EXPRESS

Figure 4(c,g,k) shows B-scan Doppler OCT flow measurements. Due to the reduced transverse velocity components, the velocity dynamic range has increased to a maximum flow rate of 76-127 mm/s (depending on the Doppler angle). This is consistent with the theoretical estimate of roughly 100 mm/s (double the M-scan Doppler flow limit). Deviations of the velocity increase with increasing $\theta$ values, as the phase shift approaches a constant value at lower discharge rates. Due to non-uniformity of the flow, transverse components at all depths cannot be simultaneously suppressed. This method performs similar to the M-scan DLS-OCT.

Figure 4(d,h,l) shows the results obtained using B-scan DLS-OCT. It has by far the highest velocity dynamic range yielding a maximum flow rate of up to 250 mm/s and a maximum speed that is unaffected by the Doppler angle, as long as the fringe washout limit is not reached. The theoretical maximum measurable velocity according to Eq. (5) and (6) and (13) and (14) is approximately 230 mm/s. This is consistent with our observation of a flow limit around 250 mm/s.

The measured profiles are in good agreement with analytical predictions, especially for $\theta = 0.94°$. However, since the flow cell is tilted, the refracted beam travels at an angle to the surface normal and with a small offset from the half-width. Therefore, for different experiments, deviations from the theoretical profiles are expected. Slightly increased noise in high flow rates for $\theta = 0.94°$ is caused by an insufficient B-scan speed that isn't set exactly at the mid-range flow velocity. Insufficiently fast scanning is not an issue for $\theta = 0.39°$ and $\theta = 1.58°$, because for these angles the measured velocities are slightly lower due to probing a different position in the flow.

To compare all flow methods simultaneously all measured velocities at a fixed angle are plotted against the expected velocities in Fig. 5(a-c). The black dashed curve corresponds to the expected value. For all angles, B-scan DLS-OCT follows the expected flow up to 250 mm/s. The second best method is B-scan Doppler OCT. This shows consistent flow measurements up to 76-152 mm/s, depending on the angle. Its accuracy gets worse for larger Doppler angles. M-scan DLS-OCT measurements have a dynamic range from zero up to 101-127 mm/s and are less dependent on the angle. M-scan Doppler OCT measurements level off at a maximum flow rate of 51 mm/s.

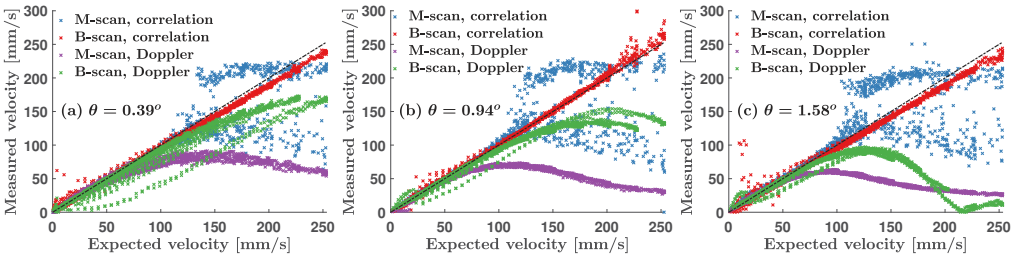


**Fig. 5.** Measured versus expected flow velocities for all methods for (a) $\theta = 0.39°$, (b) $\theta = 0.94°$, and (c) $\theta = 1.58°$.

With increasing $\theta$, M-scan and B-scan Doppler measurements deviate from the expectations at lower velocities. For the M-scan DLS-OCT measurements, the fit error becomes very large after reaching the limiting velocities. It is only the B-scan DLS-OCT measurements that show a linear behaviour for all considered flow rates. It worth noting that the B-scan methods have the same sensitivities at the highest and lowest flow speeds where the apparent velocities (due to scanning) are equal. Therefore, for these methods, higher errors are expected near the minimum and maximum flow velocities, which are visible in Fig. 5.

Optics EXPRESS

### 4.2. Omnidirectional flow measurements

Figure 6 shows the applicability of our method to the general situation of flow under non-zero Doppler angle and non-aligned B-scanning. Flow is measured in B-scan mode for discharge rates of 1/5 and 1/6 mL/s. The angle between the transverse projections of scan and flow directions, $\varphi_t$, was approximately 10° and $\varphi_z$ was unknown. For each flow rate, 5 different scan speeds were used. For the purpose of comparison with the ideal scanning assumption, $\theta$ was also determined experimentally and found to be 1.5°.

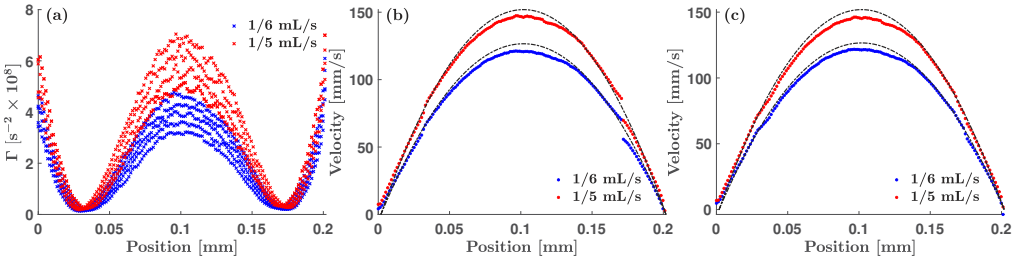


**Fig. 6.** B-scan DLS-OCT flow measurements with arbitrary scan and flow directions. (a) Obtained decorrelation parameter, $\Gamma(z)$. (b) Flow profiles obtained without any assumption on the angles, averaged over all B-scan rates. (c) Velocity profiles obtained using the small angle assumption with $\theta = 1.5°$.

Figure 6(a) shows the fitted decorrelation parameter, $\Gamma(z)$, for every scan speed and flow rate. The variation in the magnitude of $\Gamma(z)$ for the same flow rate is due to different scan speeds used. Due to the non-aligned scanning the dips in the $\Gamma(z)$ are smoothed out as compared to Fig. 3(b). Figure 6(b) shows the flow profile obtained by solving the overdetermined system of equations for $\Gamma(z)$ without any assumptions on the angles. Uncertainties in velocity are highest at the positions of the two minima. At these positions, the system of equations is underdetermined because there is a very little variation in fitted decay rates for different scan speeds. As a result, multiple solutions for $v_0(z)$ could be possible at these locations leading to slightly wrong values. Outside of these locations the velocity profile is correctly estimated.

For comparison, flow profiles were also determined from the same data using $\cos\varphi_t \approx 1$, $\varphi_z + \theta \approx \theta$ and $\theta = 1.5°$. As can be seen from Fig. 6(c), the obtained profiles match well with the ones determined without any assumptions. This suggests that $\varphi_t$ of around 10° degrees is still sufficiently small as to not violate the small angle approximation. The obtained results show that omnidirectional velocity profiles unambiguously can be determined without any underlining assumptions on the geometry if multiple B-scans are performed. The absence of any assumptions or careful alignment only requires the acquisition multiple B-scans and, hence, a longer acquisition time.

## 5. Discussion

Our results show that using B-scan DLS-OCT, aided with numerical data alignment, the transverse flow velocity dynamic range can be significantly increased. Moreover, our method works for arbitrary flow direction. The advantage of our method is in situations where the M-scan decorrelation limit is reached, where the Doppler angle is low, and the fringe washout limit is not reached.

For well-aligned B-scan DLS-OCT flow measurement there are minor deviations for Doppler angles of $\theta = 0.39°$ and $\theta = 1.58°$ from the theoretically calculated flow profiles. This is attributed to the uncertainties in the beam waist calibration, beam offset from the center and its alignment with the flow, as well as the pump stability. During the waist calibration measurement the beam

Optics EXPRESS

moves over a tilted flow cell by the B-scan distance. This alters the Gaussian beam distribution within the flow cell during the scan due to the varying sample geometry [17]. Therefore, the fitted waist, which is assumed to be constant over the scan length, slightly varies over the length of the scan. This is by far the largest source of error and can be minimized by decreasing the scan distance and/or lowering the objective NA. Another source of uncertainty is the pump stability. Lastly, the position of the sample arm beam can be less than ideal. In our analysis we assumed that the beam is positioned at the center of the flow cell in both directions. Deviations in the alignment would alter the measured flow profiles within the cell. This source of error is more severe for the B-scan methods where stationarity of the flow and diffusion dynamics along the scan is assumed.

The obtained velocity results show that the fringe washout axial velocity limit had not been reached during the experiments. B-scan DLS-OCT can measure higher flows in any geometry compared to conventional M-scan Doppler-OCT, M-scan DLS-OCT, and B-scan Doppler OCT. The optimal choice of the scan speed is important for improving the flow imaging range. The largest gain is made when the effective scan speed is in between the maximum and minimum flow speeds. In this case, according to Eq. (14), the maximum measurable velocity limit is at least factor 2 times higher. For the most simple analysis, the scan direction must be sufficiently close to the flow direction. However, it is worth noting that the small angle assumption produces correct results for angles as much as $10^{\circ}$, underlining the robustness of the method. A limitation of the method is that the flow should be uniform over the scan distance with the assumption of stationarity. Hence, the method is most appropriate for somewhat larger vessels where the diameter is much larger than the scan range. On the other hand, the scan range can be chosen arbitrarily small, while being limited by the inertia of the galvos to obtain a constant speed over small scan ranges.

Implementation of the more general case of arbitrary scan angle shows that the fitted decorrelation parameters at certain depths cannot be well determined from the measurements at different scan speeds. This is caused by the fact that the system of equations is underdetermined at those locations. This error can be decreased by increasing the number of scan velocity measurements or by fitting the velocity and angles at each depth separately [5] (instead of fitting the whole velocity profile and angles simultaneously). The latter would require a significantly larger number of B-scans, because in this case the depth-resolved equations need to be solved independently. It is worth noting that the accuracy of B-scan DLS-OCT is higher when using the Doppler angle as a fixed parameter. The Doppler angle multiplies the alignment angles from Eq. (8) and (9), increasing the fit error.

Our method for arbitrary scan angles can be applied for determining the transverse and axial velocity components in omnidirectional flows as neither the Doppler angle nor the $\varphi_t$ and $\varphi_z$ angles need to be zero. For finding the individual transverse flow components in the $x$- and $y$-directions, multiple scans in at least two linearly independent directions must be performed [5]. Our method accuracy increases with more scans at the expense of measurement time. Even when scanning at an angle with respect to the flow, it can access velocity ranges inaccessible by conventional techniques. However, it is important to note that the scan component perpendicular to the flow direction accelerates the decorrelation and adversely affects the maximum measurable velocity limits. Therefore, to achieve the highest flow measurement gain, scanning along the flow direction is favorable. Any flow measurement gain is achieved when the decorrelation reduction due to the scan component along the flow is higher than the above-mentioned decorrelation penalty.

The numerical alignment is essential in implementing B-scan DLS-OCT methods and it minimizes $\varphi_z$. In principle, the OCT signal needs to be normalized by the confocal response and sensitivity roll-off before performing the numerical alignment. For typical flow geometries with relatively low tilt angles, these functions are slowly varying at the length scales of voxel shifts

Optics EXPRESS

and the normalization can be dropped. However, in the limit of high axial velocities, the fringe washout causes a significant decrease in the signal level [7].

Another important application of the B-scan correlation analysis is improving the accuracy in measuring the diffusion coefficient of flowing particles from their decorrelation. This is of particular importance for in-line particle sizing during process control [21]. Estimation of the diffusion coefficient under flow using the M-scan DLS-OCT becomes problematic when the flow decorrelation is at a similar rate as the diffusion decorrelation or when it entirely dominates the decorrelation [8]. This is a problem in particular for high flow rates and/or slow diffusion (large particles). By scanning along the flow, the effective flow decorrelation is minimized and the diffusion coefficient can be determined more accurately. For fast flowing suspensions in the channel, estimation of the diffusion coefficient is only possible very close to the channel walls, in a limited number of depth voxels, where the flow velocity is low. However, a close proximity to the walls creates additional unwanted effects for particles (stickiness, particle-wall interactions) and their behaviour deviates from the free diffusion. When scanning along the flow, these limitations can be removed. First, the apparent flow velocity can be minimized not near the walls but well inside the channel. These locations depend on the combination of flow and effective scan speeds. Second, the number of depth voxels where the flow decorrelation is minimal can be more than doubled.

Figure 7 shows the obtained normalized diffusion coefficients for the particles in the solution under flow for $\theta = 0.39^{\circ}$ at discharge rates of 1/30 mL/s and 1/15 mL/s. The black curves correspond to static diffusion measurements (no flow), blue curves correspond to the conventional M-scan diffusion measurements under flow, and red curves correspond to B-scan diffusion measurements under flow. The fitted diffusion coefficients are given with 95% confidence intervals indicated by the area between the two lines. For M-scan diffusion measurement the obtained diffusion coefficients become less reliable as the flow velocity increases. With the B-scan measurements, $D$ can be estimated accurately inside the channel further away from its walls indicated by the arrows and with a higher accuracy at more depth voxels than in the M-scan mode. The advantage of our method is greater with faster flows and for samples with a larger diffusion coefficient. The measured diffusion coefficient is most accurate when the B-scan angle is aligned with the flow direction and the numerical alignment is not required. If the latter cannot be avoided, the frequency domain alignment is preferred to the spatial alignment.

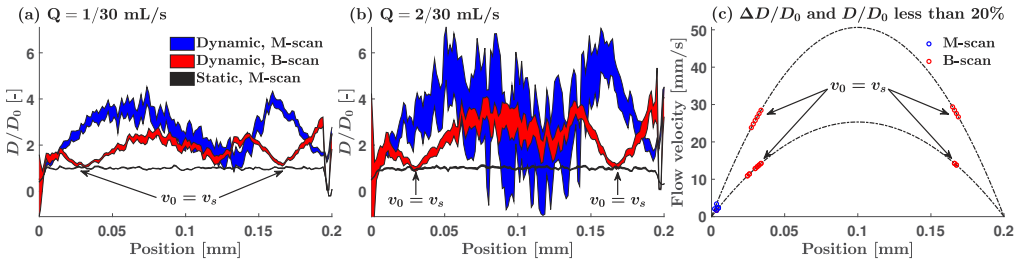


**Fig. 7.** Diffusion estimation under static and flow conditions with or without scanning. (a) Normalized diffusion coefficient for 1/30 mL/s discharge rate. (b) Normalized diffusion coefficient for 1/15 mL/s discharge rate. The areas in the curve represent 95% confidence intervals. The locations where the effective scan speed equals the flow speed are indicated. (c) Locations in the flow profile where the relative error of the diffusion coefficient is less than 20%.

Optics EXPRESS

## 6. Conclusion

We have implemented the B-scan correlation-based DLS-OCT method for measuring omnidirectional flows. Our method extends the maximum measurable velocity limit by at least a factor of 2 compared to the standard M-scan DLS-OCT or Doppler OCT techniques. We have shown that our method can be applied to flow geometries where a proper scan alignment is not possible. In addition, we have demonstrated that the suggested method can be used to estimate a diffusion coefficient more accurately under flow conditions.

**Funding.** Nederlandse Organisatie voor Wetenschappelijk Onderzoek Domain Applied and Engineering Sciences (17988).

**Acknowledgments.** We would like to thank InProcess-LSP for their support and discussions.

**Disclosures.** The authors declare no conflicts of interest.

**Data availability.** Data underlying the results presented in this paper and the relevant analysis routines are available at [22].

## References

1. J. Kalkman, R. Sprik, and T. G. van Leeuwen, "Path-length-resolved diffusive particle dynamics in spectral-domain optical coherence tomography," Phys. Rev. Lett. **105**(19), 198302 (2010).
2. J. Walther and E. Koch, "Flow measurement by lateral resonant Doppler optical coherence tomography in the spectral domain," Appl. Sci. **7**(4), 382 (2017).
3. N. Weiss, T. G. van Leeuwen, and J. Kalkman, "Localized measurement of longitudinal and transverse flow velocities in colloidal suspensions using optical coherence tomography," Phys. Rev. E **88**(4), 042312 (2013).
4. J. Lee, W. Wu, J. Y. Jiang, B. Zhu, and D. A. Boas, "Dynamic light scattering optical coherence tomography," Opt. Express **20**(20), 22262–22277 (2012).
5. B. K. Huang and M. A. Choma, "Resolving directional ambiguity in dynamic light scattering-based transverse motion velocimetry in optical coherence tomography," Opt. Lett. **39**(3), 521–524 (2014).
6. X. Liu, Y. Huang, J. C. Ramella-Roman, S. A. Mathews, and J. U. Kang, "Quantitative transverse flow measurement using OCT speckle decorrelation analysis," Opt. Lett. **38**(5), 805–807 (2013).
7. H. C. Hendargo, R. P. McNabb, A. Dhalla, and J. A. Izatt, "Doppler velocity detection limitations in spectrometer-based versus swept-source optical coherence tomography," Biomed. Opt. Express **2**(8), 2175–2188 (2011).
8. N. Weiss, T. G. van Leeuwen, and J. Kalkman, "Simultaneous and localized measurement of diffusion and flow using optical coherence tomography," Opt. Express **23**(3), 3448–3459 (2015).
9. N. Uribe-Patarroyo, M. Villiger, and B. E. Bouma, "Quantitative technique for robust and noise-tolerant speed measurements based on speckle decorrelation in optical coherence tomography," Opt. Express **22**(20), 24411–24429 (2014).
10. E. Koch, J. Walther, and M. Cuevas, "Limits of Fourier domain Doppler-OCT at high velocities," Sens. Actuators, A **156**(1), 8–13 (2009).
11. N. Uribe-Patarroyo, A. L. Post, S. Ruiz-Lopera, D. J. Faber, and B. E. Bouma, "Noise and bias in optical coherence tomography intensity signal decorrelation," OSA Continuum **3**(4), 709–741 (2020).
12. T. W. Taylor and C. M. Sorensen, "Gaussian beam effects on the photon correlation spectrum from a flowing Brownian motion system," Appl. Opt. **25**(14), 2421–2426 (1986).
13. M. G. O. Gräfe, M. Gondre, and J. F. de Boer, "Precision analysis and optimization in phase decorrelation OCT velocimetry," Biomed. Opt. Express **10**(3), 1297 (2019).
14. B. J. Berne and R. Pecora, *Dynamic Light Scattering* (Dover Publications, 2000).
15. C. S. Johnson and D. A. Gabriel, *Laser Light Scattering* (Dover Publications, 1994).
16. D. P. Chowdhury, C. M. Sorensen, T. W. Taylor, J. F. Merklin, and T. W. Lester, "Application of photon correlation spectroscopy to flowing Brownian motion systems," Appl. Opt. **23**(22), 4149–4154 (1984).
17. R. R. Vardanyan, V. K. Dallakyan, U. Kerst, and C. Boit, "Laser beam transmission and focusing inside media," J. Contemp. Phys. **46**(5), 218–225 (2011).
18. H. Bruus, "Acoustofluidics 1: Governing equations in microfluidics," Lab Chip **11**(22), 3742–3751 (2011).
19. J. Kalkman, "Fourier-domain optical coherence tomography signal analysis and numerical modeling," Int. J. Opt. **2017**, 1–16 (2017).
20. S. H. Yun, G. J. Tearney, J. F. de Boer, and B. E. Bouma, "Motion artifacts in optical coherence tomography with frequency domain ranging," Opt. Express **12**(13), 2977–2998 (2004).
21. R. Besseling, M. Damen, J. Wijgergans, M. Hermes, G. Wynia, and A. Gerich, "New unique PAT method and instrument for real-time inline size characterization of concentrated, flowing nanosuspensions," Eur. J. Pharm. Sci. **133**, 205–213 (2019).
22. K. Cheishvili, "Scanning DLS-OCT data and analysis routines," Zenodo (2022), https://doi.org/10.5281/zenodo.6425084.